

Electrochemical Synthesis of Large Area MoO₂ Nanosheets and their Photocatalytic Activity

GUBRAN ALNAGGAR, K.R. RAKSHA and S. ANANDA*

Department of Studies in Chemistry, University of Mysore, Manasagangotri, Mysore-570006, India

*Corresponding author: Tel: +91 821 2419663; E-mail: snananda@yahoo.com

Received: 19 July 2018;

Accepted: 30 September 2018;

Published online: 31 December 2018;

AJC-19209

Monoclinic molybdenum dioxide (MoO₂) nanosheets have been successfully synthesized by a simple electrochemical method. The as prepared MoO₂ was used as a photocatalyst for the photocatalytic degradation of Indigo carmine dye under various experimental conditions and also as oxygen evolution catalyst for the decomposition of potassium permanganate. Initially, as-prepared MoO₂ was characterized by different techniques namely, X-ray diffraction, scanning electron microscopy FE-SEM, UV-visible and FT-IR techniques, so as to study and revealed the morphological, structural, functional and optical properties. The results revealed that photocatalyst has nanosheets morphology with thickness less than 10 nm and it has also monoclinic crystal structure with an average crystallite size of 27 nm. The optical properties studies showed that band gap (E_g) value of MoO₂ (3.85 eV) lies in the UV region and can be a suitable candidate for UV light photocatalytic application. In addition, the experimental results revealed an excellent photocatalytic performance of MoO₂ in the degradation of Indigo carmine under UV light irradiation and also for the decomposition of KMnO₄ by oxygen evolution reaction.

Keywords: Electrochemical method, Molybdenum dioxide nanosheets, Band gap, Photocatalysis.

INTRODUCTION

Although molybdenum has oxidation states ranging from +2 to +6, among them, two forms of oxides are existing mainly *i.e.*, Mo(IV) and Mo(VI) oxide. The presence of free electrons in the valance band region enhances the catalytic activity of Mo⁴⁺ in MoO₂ unlike Mo⁶⁺ in MoO₃, where all the valence electrons of the metal are covalently bonded to neighbouring oxygen atoms [1-5]. MoO₂ nanostructure has more advantages than bulk MoO₂ because it exhibits high surface area leading to increasing the number of active sites available to the reaction and enhances the applications [6-12]. To date, many morphologies of MoO₂ nanostructures have been synthesized such as nanowires arrays, hollow fibres, hollow spherical and others morphologies [1,3,7-10,12-19]. Among the different morphologies of MoO₂ nanostructure, MoO₂ nanosheets have significance chemical, physical, electronic and optical properties which make them favourable candidates for a wide range of application such as photocatalytic reactions [6,7,9,11,17,19,20].

Nanosheets are highly advantageous for enhancing the efficiency of photocatalysis reaction due to (a) the large specific surface area which provides a plenty of reactive sites; (b) the

short bulk diffusion length which reduces the recombination possibility of photoexcited charge carriers; (c) the most important advantages are increasing the band gap and changing the photophysical properties of charge carriers resulting from the quantum confinement effect, which can play a vital role in extending the lifetime of charge carriers [6]. Generally, 2D nanosheets are synthesized using chemical vapour deposition (CVD), which it has considered one of the most used methods for preparing of nanosheets materials [7,9,21]. However, CVD has complicated and expensive procedure and requires high temperature and vacuum. Till now, there are few studies about the synthesizing of MoO₂ nanosheets structure [11,17,19,20]. To the best of our knowledge there is no report on synthesis of MoO₂ sheet using electrochemical method. The major advantages of the electrochemical methods based in that nanoparticles can be obtained with high purity and also nanoparticles size can be controlled by adjusting the density of current without a need for high cost equipment or vacuum [12,22]. Herein, large area of monoclinic MoO₂ nanosheets were successfully obtained for first time *via* simple electrochemical method and investigated as catalyst for the degradation of organic and inorganic materials.

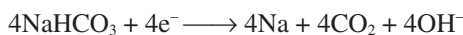
EXPERIMENTAL

Molybdenum metal wire 99.95 % (metal basis), sodium bicarbonate and Indigo carmine dye are procured from Alfa Aesar Pvt. Ltd., platinum electrode from Elico Pvt. Ltd. All the chemicals were used without further purification. Deionized water was produced by a PURELAB Ultra-water purification system.

Synthesis: The electrochemical synthesis experiments were carried out in stationary conditions and in an open system (The electrolyte in contact with air and atmospheric humidity), using a DC power supply (0-60 V) and a two electrode configuration. Pure Mo wires have been used as anode; surface of the electrode was mechanically polished with finer grade emery paper then rinsed in distilled water and finally dried, and a round platinum as cathode. The experiment was performed with 20 mL of sodium bicarbonate (5 %) and the area between the electrodes was about 1.5 cm. The sodium bicarbonate was used as a conductive salt and also employed as oxides source. A potential difference of 7 V was applied between the electrodes using a DC power supply. Current densities were between 20 and 30 mA cm⁻² applied at electrolyte temperatures in the range of 20-30 °C for durations between 20 and 24 h without stirring.

After Mo anode dissolution, 20-40 mL of water has been added to the electrolyte. The obtained white precipitate has been washed with deionized water and ethanol and then subjected to centrifugation at 2000 rpm for 20 min. This sequence has been followed by drying at 105 °C for 1 h and calcinations at 600 °C for 1 h to obtain nanosheet-MoO₂ powder.

Possible formation mechanism of MoO₂: The formation process for MoO₂ nanosheet may be supposed as follow:



Characterization: The as-prepared MoO₂ nanosheets were identified by X-ray diffraction method using Rigaku Miniflex II desktop X-ray diffractometer (CuK_α radiation = 1.54 Å) employing a scan rate of 0.02°/s range from 0° to 80°. The morphology of as prepared nanosheets was analyzed by scanning electron microscopy (SEM-EDX) from Quanta-200 FEI, Netherlands. FT-IR spectrum was recorded using JASCO FTIR with wave number ranging from 4000 to 500 cm⁻¹. The optical properties for as-prepared MoO₂ nanosheets were studied by UV-visible spectrophotometer at room temperature with JASCO-UV VIS spectrophotometer. The scanning range was from 200 to 800 nm with an interval of 1 nm.

Photocatalytic study: In the photocatalytic study, Indigo carmine dye was representing as an organic pollutant dye in wastewater. For photocatalytic experiments, a tungsten-halogen lamp (50 W) was used as UV light source, which was placed at about 15 cm away from the solution. In a typical UV-light photocatalytic experiment, the effect of varying catalyst dosage (0.5, 3, 5, 10 and 20 mg of as-prepared MoO₂ nanosheets) and initial dye concentrations (5, 10, 15, and 20 mg L⁻¹ of Indigo carmine dye (20 mL)), were studied and optimized. Before irradiation, the suspension was magnetically stirred for 0.5 h in the dark to ensure an adsorption-desorption equilibrium was established

at the surface of photocatalyst. The absorbance behaviour of Indigo carmine dye was recorded for different time intervals.

So as to estimate the degradation efficiency fulfilled throughout the treatment, the COD was measured. In present work, the total quantity of oxygen required for oxidation of organic matter to CO₂ and H₂O was carried out, the COD of dye solution was estimated before and after treatment (using K₂Cr₂O₇ oxidation method). The photodegradation and COD efficiency was calculated [23-25] by the following eqns. for all the photocatalytic experiments.

$$\text{Photocatalytic efficiency (D)} = \frac{A_0 - A}{A_0} \times 100 \% \quad (1)$$

where A₀ and A are the absorbance of dye solution before and after illumination, respectively.

COD as mg/L of oxygen consumed =

$$\frac{(A-B) \times \text{Normality of FAS} \times 8000}{\text{mL of sample taken}} \quad (2)$$

where, A = FAS used for titration of blank (mL) and B = mL. FAS used for titration of sample (mL), FAS = ferrous ammonium sulfate.

RESULTS AND DISCUSSION

Structure properties and morphology: The SEM morphologies of as-prepared MoO₂ nanosheets are shown in Fig. 1. It is clear that MoO₂ has nanosheet morphology with thickness less than 10 nm. The images also show that MoO₂ possesses mesoporous structure. The porous appears clearly in SEM images (marked with white arrow). It is well known that the size of nanosheet prepared by chemical methods is usually very small. However, in present case the sheet has large surface that leads to increases the surface area. Increasing surface area is associated with an increase in the number of photocatalyst sites and thereby the photocatalytic activity.

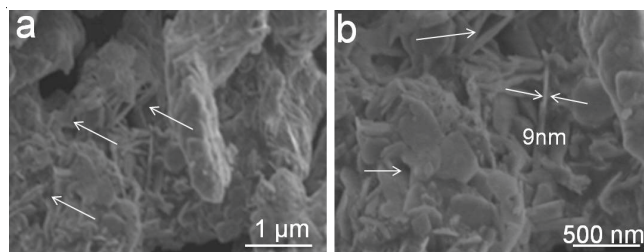


Fig. 1. FE-SEM image of as prepared MoO₂ nanosheets (a) low and (b) high magnification

The X-ray diffractogram of as-prepared MoO₂ nanosheet (Fig. 2) showed the reflection peaks at Bragg angle 2θ which appeared due to (-111), (101), (210), (212), (202), (-301), (-312), (-233), (-303), (310), (-321), (-402), (-413) and (-233) planes. All the diffraction peaks can be assigned to MoO₂ with monoclinic structure with a lattice parameter a = 5.65 Å, b = 4.86 Å, c = 5.645 Å, β = 120.941 Å, according to (JCPDS 032-0671) with a space group of P21/c [19,20,26]. The average crystallite size D was found to be 27 nm from the XRD pattern using the Scherrer equation:

$$D = \frac{0.94\lambda}{B \cos \theta}$$

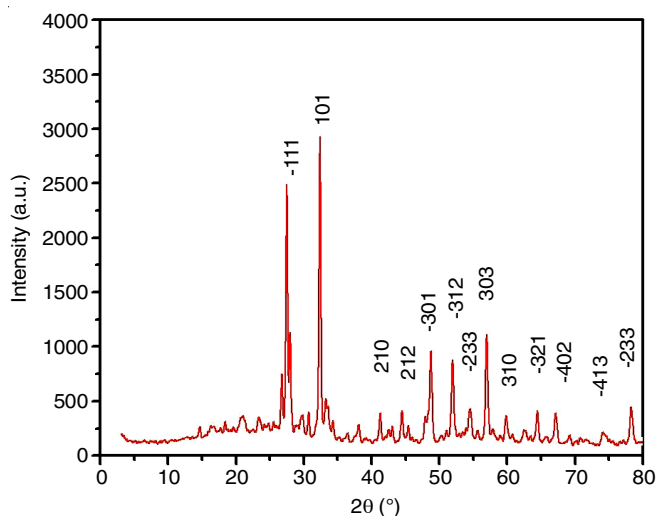


Fig. 2. XRD pattern of as prepared MoO₂ nanosheets

where λ is the wavelength of X-ray source and B is the full width at half maximum of individual peak at 2θ (where θ is the diffraction angle). $k = 0.94$, and $\lambda = 1.54056 \text{ \AA}$.

Noticeably, the (101) peak intensity is high compared to that in the standard of monoclinic MoO₂ [19,26]. That indicates MoO₂ has grown along (101). This is in agreement with SEM results. The MoO₂ has nanosheets structure generally grows along (101) direction [19].

According to the facets theorem of Wulff, at equilibrium, the crystal formed has to be confined by planes to minimize the total surface energy. The close-packed plane (CPP) for MoO₂ is (010) and the second CPP is (101). So (010) and (101) planes have lower surface energy and larger surface area, resulting in the preference of growth along (010) and (101) directions. As a result the obtained morphology of crystals is sheet-like structure with lower surface energy [19].

The FT-IR spectra of as-prepared MoO₂ nanosheet is shown in Fig. 3. The sharp peaks appeared at 1450 and 1650 cm⁻¹ were ascribed to the vibrational of hydrogen in hydroxyl group in Mo-OH and H-O-H, respectively [12,27], also the clear sharp band noticed at 3330 cm⁻¹ represented the stretching mode of absorbed water [12,28]. The presence of these peaks gives clear evidence to hydrous property of as-prepared MoO₂ nanosheet. The intense peak at 830 cm⁻¹ and small peaks at 695 cm⁻¹ were due to asymmetric stretching vibrations of O-Mo-O short-length and medium-length bands, respectively [12,29].

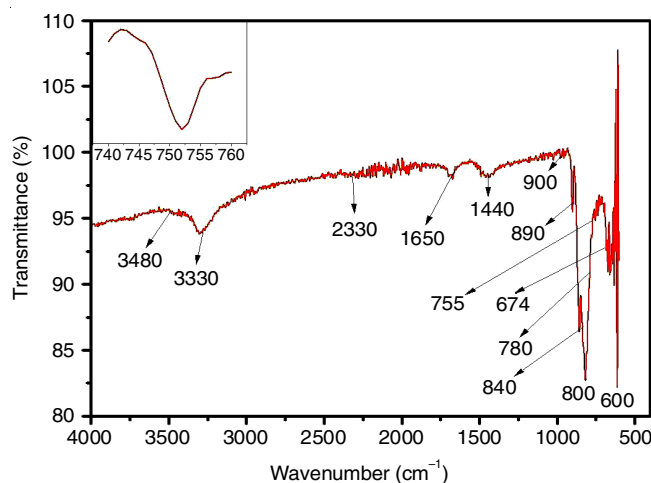


Fig. 3. FT-IR spectra of as prepared MoO₂ nanosheets

The absorption peak which appears at around 650 cm⁻¹ was attributed to the vibration mode of Mo-O-Mo bonds [12, 27,29]. The monoclinic structure has confirmed by the small peaks at 750 cm⁻¹, this peak was ascribed to the characteristic stretching vibration mode of Mo-O [12,18]. The other peaks at about 2300, 3500 and 1600 cm⁻¹ could be attributed to the absorbed water and carbon dioxide molecules [12,17,27].

Optical properties study: To gain further information about the as prepared MoO₂ nanosheet, the optical properties studies were carried out. The UV-visible spectrum shown in Fig. 4a revealed that as-prepared MoO₂ nanosheets show maximum intensity peak at 293 nm in the UV region and there are no absorption peaks in the visible region. Furthermore, direct band gap of MoO₂ was calculated from tauc plot (Fig. 4b) to be 3.85 eV. The obtained high band gap value compared to the reported value of another morphologies [10], demonstrated that as prepared product has nanosheets morphologies which have small thickness (less than 10 nm as its clear in SEM image). The increasing in band gap value can be attributed to the distance shifting between conduction and valance band edges as a result of quantum confinement effect [6]. However, the obtained band gap value is in agreement with literature [18].

A linear rise near the absorption edge confirms the direct nature of transition. This UV-visible result implies that as-prepared MoO₂ will show photocatalytic activity under UV irradiation.

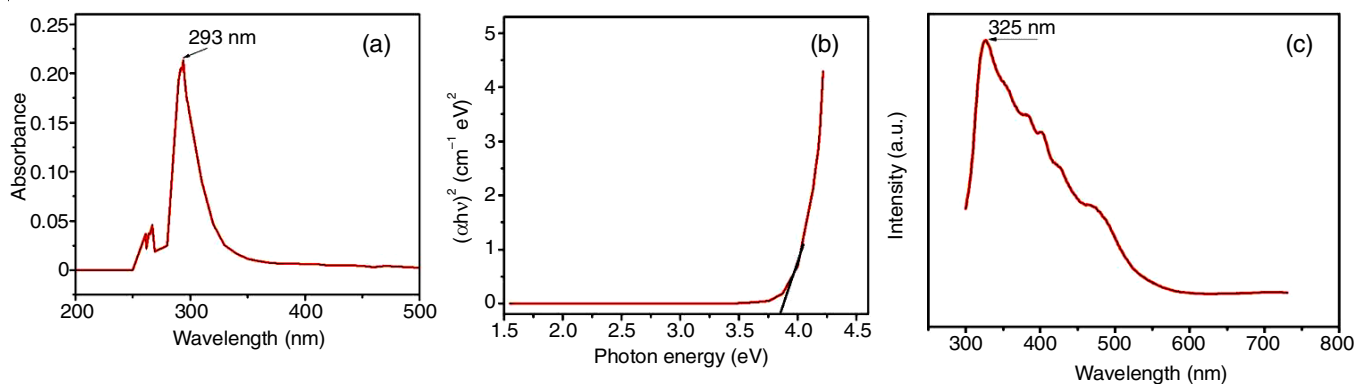


Fig. 4. (a) UV-visible spectra of as prepared MoO₂ nanosheets (b) Tauc's plot (c) Photoluminescence spectra of as prepared MoO₂ nanosheets

Fig. 4c shows the photoluminescence spectrum of as-prepared MoO₂ nanosheet excited by 337 nm wavelength at room temperature. Photoluminescence plays a vital role in the photocatalytic degradation, the high photoluminescence intensity, the high recombination rate of the charge carriers [25,30]. It is found that the emission peaks were appeared at 455, 420, 396 and 380 nm with the maximum emission peak at 325 nm. The semiconductor properties have confirmed due to the presence of a strong absorption peaks around 300 nm. The maximum absorption peak is very close to that value obtained from tauc plot. So this peak is ascribed to direct transition from the valance band to conduction band that means band gap value has confirmed by photoluminescence spectrum. The other peaks observed in photoluminescence spectrum may be due to the presence of some impurities or defects in the prepared nanosheets structure [18,19,31].

Photodegradation of Indigo carmine dye: The photocatalytic activity of as-prepared MoO₂ nanosheets has been studied by using Indigo carmine dye as organic pollutants. Indigo carmine dye is a rather toxic dye which is used in the industry mainly in the field of denim textile production. The contact with Indigo carmine dye may irritate skin and eye. Likewise, it can cause damage to the conjunctiva and cornea. It is well-known that Indigo carmine dye can cause acute toxicity and it is considered a cancer-causing chemical as well. In addition, it has been demonstrated that consumption of the dye causes tumour. For all the reasons mentioned above, the releasing of Indigo carmine dye should be followed by treatment, otherwise it will be very harmful. In addition, Indigo carmine dye has strong stability and symmetrical structure, so that its degradation would not be easy. Thus, recent researches take cognizance of the removal of Indigo carmine dye containing wastewaters [22,24].

Effect of initial dye concentration: To get information about the dye dependent photocatalytic degradation, the concentration of Indigo carmine dye was varied. Fig. 5a shows the effect of dye initial concentration on photocatalytic degradation, as initial dye concentration increase, degradation rate and degradation

efficiency were decreased. The former can be donated as the degradation rate is determined by the formation of hydroxide radical, which reacts with the dye molecules. As the initial dye concentration increase, more dyes molecules are available for excitation and energy transfer and the majority of active sites would be covered, then the formation of hydroxide radicals decreases which leads to the decrease in degradation rate. The latter could be ascribed to that high dye concentration, the less light penetration, the fewer photons reach the active sites of catalysts. As a results, the production of free radicals species like hydroxyl and superoxide decreases then the degradation efficiency decreases [22,32,33]. The rate of degradation reaction with respect to dye concentration is shown in Table-1.

Effect of catalyst dosage: To get more details about the effect of catalyst dosage in both degradation rate and efficiency, the concentration of photocatalyst MoO₂ nanosheets were varied at (0.5, 3, 5, 10 and 20 mg) keeping the dye concentration constant and the influence of Indigo carmine dye photodegradation was studied. The T % was recorded upon UV light illumination every 10 min as shown in Fig. 5b. Fig. 5b illustrates the effect of different amounts of as-prepared MoO₂ nanosheets on the decomposition of dye molecules. As the initial catalyst dosage increases, the degradation rate increases up to a $4.43 \times 10^{-5} \text{ S}^{-1}$ and then declines, the degradation efficiency also increases up to a maximum value 94.3 % and then decreases. Initially, an increase in the initial catalyst dosage leads to increase in the number of active sites on catalyst surface available for the reaction and more dyes molecules can be absorbed, hence the degradation rate and efficiency would increase up to limit. Beyond this point the degradation rate was decreased with the increment of catalyst dosage which could be ascribed to screen effect and light scattering as a results to agglomeration of the particles which led to the decrease of surface area [22,25,30,32-34].

On the other hand, the decrease in degradation efficiency may be ascribed to the decrease in the light penetration with catalyst increment. An increment in catalyst dosage makes the

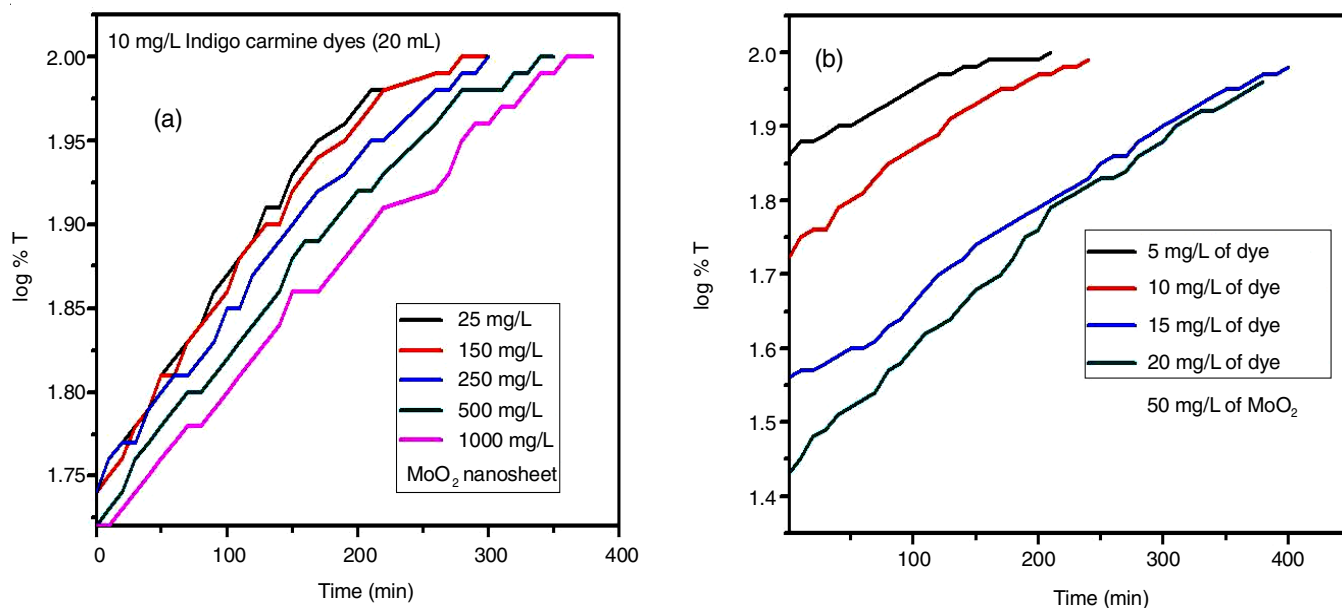


Fig. 5. (a) Plot of log % T vs. time for different amount of catalyst and (b) different initial dye concentration

TABLE-1
EFFECT OF CATALYST DOSAGE AND INITIAL DYE CONCENTRATION ON THE DEGRADATION RATE

Catalyst dosage (mg)	Concentration of dyes (mg/L)	Reaction rate K (s ⁻¹)	Time taken for complete degradation (min)	COD values (mg L ⁻¹)		Degradation efficiency (%)
				Before degradation	After degradation	
50	5	5.41 × 10 ⁻⁵	210	192	4	97.91
	10	4.43 × 10 ⁻⁵	250	320	18	94.30
	15	4.28 × 10 ⁻⁵	400	448	28	93.75
	20	2.58 × 10 ⁻⁵	450	640	50	92.18
Conc. of dyes (mg/L)	Catalyst dosage (mg/L)					
10	25	3.34 × 10 ⁻⁵	300	320	32	90.00
	50	4.43 × 10 ⁻⁵	250		18	94.30
	150	3.74 × 10 ⁻⁵	300		26	91.87
	250	3.23 × 10 ⁻⁵	300		28	91.25
	500	3.13 × 10 ⁻⁵	360		40	87.50
	1000	2.99 × 10 ⁻⁵	400		40	87.50

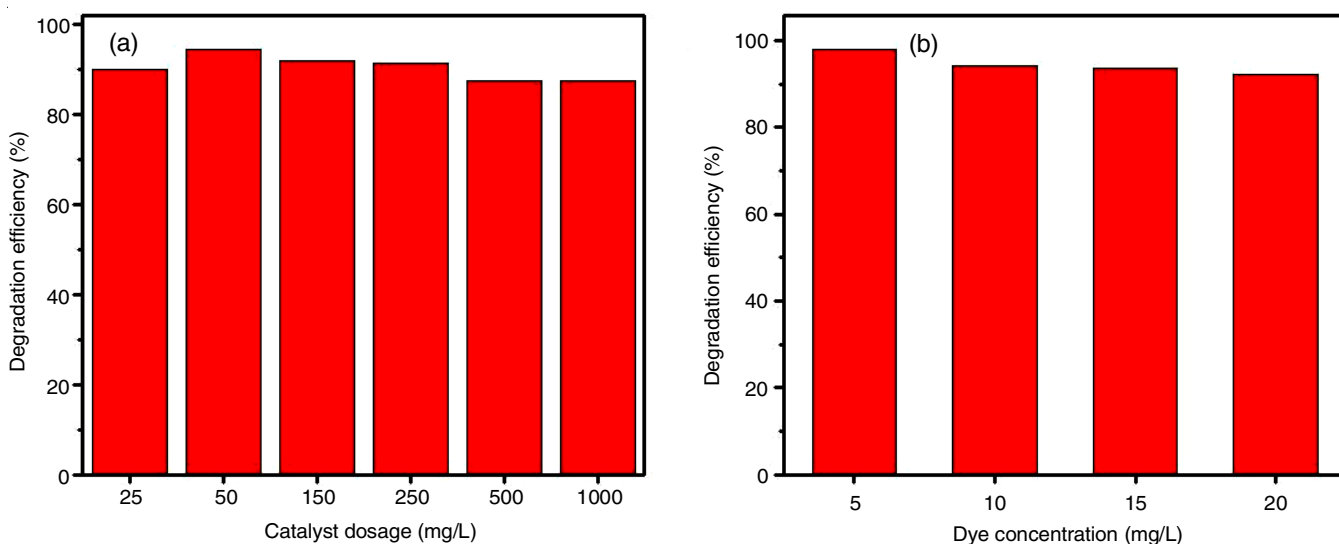


Fig. 6. (a) Effect of the different initial concentration of dye on the degradation efficiency and (b) the effect of the catalyst dosage on the degradation efficiency

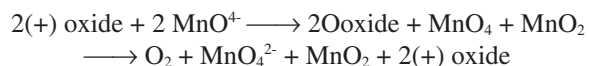
turbidity of the solution high and light penetration is hindered. Increase of catalyst dosage also leads to the deactivation of activated molecules by collision with ground state molecules [22,25,35]. It indicates that optimal catalyst dosage of as-prepared MoO₂ nanosheets is 50 mg/L. The degradation rate constant with respect to the amount of catalyst is shown in Table-1.

Decomposition of potassium permanganate: It was clarified that when the solid catalyst has more p-type character, it gives strong effect on the rate of reaction. The role of MoO₂ as a p-type semiconductor in the decomposition reaction of other materials will have considerable value in the practical significance point of view for oxygen evolution reaction.

The decomposition of KMnO₄ solution including oxygen evolution reaction, it has been suggested that during the decomposition, electrons transfer within permanganate ions with the formation of stable MnO₄²⁻ ions and unstable MnO₂ radicals.



The reaction kinetics of decomposition of KMnO₄ was performed by studying the effect of both the amount of nanosheets as p-type catalyst and the initial concentration of KMnO₄. The reaction can be illustrated as:



where O_{oxide} is an oxygen atom attracted by oxide, MnO₄ is a radical and (+) a positive hole in oxide. In the current study, an investigation has been performed to shed light on the kinetic of the reaction by which MoO₂ nanosheets will act as a catalyst for the decomposition of KMnO₄.

Effect of KMnO₄ initial concentration: In this case, the reaction was carried out by varying the concentration of KMnO₄ and keeping the amount of added catalyst constant. Fig. 7a shows the effect of KMnO₄ initial concentration on photocatalytic degradation, the increasing in KMnO₄ initial concentration leads to the decrease in reaction rate. The possible reason for that may be similar to the one mentioned above in case of Indigo carmine dye degradation. The different concentrations of KMnO₄ which were used in the experiments illustrated in Table-2.

The decomposition reaction was studied by adding different amount of catalyst to illustrate the influence of catalyst dosage in the rate of reaction. Fig. 7b shows the effect of different amounts of as-prepared MoO₂ nanosheets on the decomposition of KMnO₄ molecules, the reaction rate increases with increases in the amount

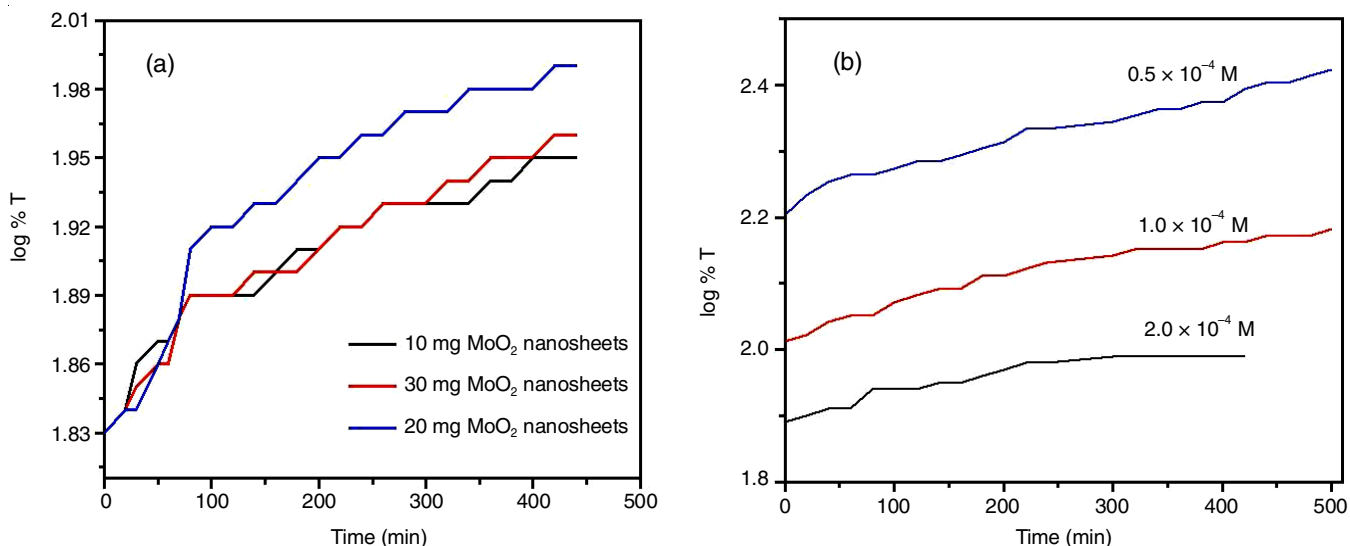


Fig. 7. (a) Plot of log % T vs. time for different amount of catalyst and (b) for different initial concentration of KMnO₄

of as-prepared MoO₂ nanosheets which can be explained in a similar way as in the case of Indigo carmine dye. The different amount of catalyst added along with rate reaction is shown in Table-2.

Catalyst dosage (mg)	Decomposition rate (S ⁻¹)
10	1.15 × 10 ⁻⁵
20	1.35 × 10 ⁻⁵
30	1.16 × 10 ⁻⁵
Initial of KMnO ₄ concentration (M)	
0.5 × 10 ⁻⁴	1.467 × 10 ⁻⁵
1 × 10 ⁻⁴	1.212 × 10 ⁻⁵
2 × 10 ⁻⁴	0.907 × 10 ⁻⁵

To conclude, the high photocatalytic activity of as-prepared MoO₂ nanosheets in the decomposition of both organic and inorganic materials can be ascribed to the quantum confinement effect as a result to nanosheets morphologies. The high surface area and larger band gap have played important role in the photocatalytic activity, the former provides a more numbers of the active sites in the surface of catalyst, which would be ready to absorb as much as possible reactant molecules the latter can contribute in delaying the recombination time of the charge carries [6,22].

Conclusion

In the present study, monoclinic MoO₂ nanosheets are synthesized using electrochemical methods. The prepared MoO₂ nanosheets exhibit large band gap 3.85 eV which can be attributed to the small thickness of MoO₂ nano-sheets through the quantum confinement effect. The small thickness of MoO₂ nanosheets leads to shift the absorption edge to lower wavelength. The obtained product shows high activity in the photocatalytic degradation of both Indigo carmine dye and potassium permanganate as organic and inorganic material, respectively.

ACKNOWLEDGEMENTS

One of the authors, Gubran Alnaggar Acknowledge UGC (BSR) DST-PURSE Programme, IOE, UPE CPEPA and University of Mysore, Mysore, India.

CONFLICT OF INTEREST

The authors declare that there is no conflict of interests regarding the publication of this article.

REFERENCES

- C.A. Ellefson, O. Marin-Flores, S. Ha and M.G. Norton, *J. Mater. Sci.*, **47**, 2057 (2012); <https://doi.org/10.1007/s10853-011-5918-5>.
- O. Marin-Flores, L. Scudiero and S. Ha, *Surf. Sci.*, **603**, 2327 (2009); <https://doi.org/10.1016/j.susc.2009.05.010>.
- X. Yang, W. Chen, Y. Liu, Y. Li and Y. Qi, *J. Mater. Sci. Mater. Electron.*, **28**, 1740 (2017); <https://doi.org/10.1007/s10854-016-5720-x>.
- M. Kumar Trivedi, *Int. J. Mater. Sci. Appl.*, **4**, 390 (2015).
- J. Baltrusaitis, B. Mendoza-Sanchez, V. Fernandez, R. Veenstra, N. Dukstiene, A. Roberts and N. Fairley, *Appl. Surf. Sci.*, **326**, 151 (2015); <https://doi.org/10.1016/j.apsusc.2014.11.077>.
- P. Niu, L. Zhang, G. Liu and H.M. Cheng, *Adv. Funct. Mater.*, **22**, 4763 (2012); <https://doi.org/10.1002/adfm.201200922>.
- Y. Zhao, Y. Zhang, Z. Yang, Y. Yan and K. Sun, *Sci. Technol. Adv. Mater.*, **14**, 043501 (2013); <https://doi.org/10.1088/1468-6996/14/4/043501>.
- B. Hu, L. Mai, W. Chen and F. Yang, *ACS Nano*, **3**, 478 (2009); <https://doi.org/10.1021/nn800844h>.
- Y. Shi, B. Guo, S.A. Corr, Q. Shi, Y.S. Hu, K.R. Heier, L. Chen, R. Seshadri and G.D. Stucky, *Nano Lett.*, **9**, 4215 (2009); <https://doi.org/10.1021/nl902423a>.
- N. Dukstiene and D. Sinkeviciute, *J. Solid State Electrochem.*, **17**, 1175 (2013).
- J. Ni, Y. Zhao, L. Li and L. Mai, *Nano Energy*, **11**, 129 (2015); <https://doi.org/10.1016/j.nanoen.2014.10.027>.
- N. Dukstiene, D. Sinkeviciute and A. Guobiene, *Open Chem.*, **10**, 1106 (2012); <https://doi.org/10.2478/s11532-012-0012-7>.
- R. Naouel, F. Touati and N. Gharbi, *E-J. Chem.*, **9**, 233 (2012); <https://doi.org/10.1155/2012/506572>.

14. D. Koziej, M.D. Rossell, B. Ludi, A. Hintennach, P. Novák, J.D. Grunwaldt and M. Niederberger, *Small*, **7**, 377 (2011); <https://doi.org/10.1002/sml.201001606>.
15. D. Sinkeviciute, J. Baltrusaitis and N. Dukstiene, *J. Solid State Electrochem.*, **15**, 711 (2011); <https://doi.org/10.1007/s10008-010-1137-2>.
16. L. Mai, F. Yang, Y. Zhao, X. Xu, L. Xu, B. Hu, Y. Luo and H. Liu, *Mater. Today*, **14**, 346 (2011); [https://doi.org/10.1016/S1369-7021\(11\)70165-1](https://doi.org/10.1016/S1369-7021(11)70165-1).
17. H. Zhang, L. Zeng, X. Wu, L. Lian and M. Wei, *J. Alloys Compd.*, **580**, 358 (2013); <https://doi.org/10.1016/j.jallcom.2013.06.100>.
18. Z. Xiang, Q. Zhang, Z. Zhang, X. Xu and Q. Wang, *Ceram. Int.*, **41**, 977 (2015); <https://doi.org/10.1016/j.ceramint.2014.09.017>.
19. X. Liu, Y. He, S. Wang and Q. Zhang, *J. Alloys Compd.*, **509**, S408 (2011); <https://doi.org/10.1016/j.jallcom.2011.01.089>.
20. H. He, Y. Man, J. Yang, J. Xie and M. Xu, *R. Soc. Open Sci.*, **4**, 170892 (2017); <https://doi.org/10.1098/rsos.170892>.
21. C. Tan, Z. Lai and H. Zhang, *Adv. Mater.*, **29**, 1701392 (2017); <https://doi.org/10.1002/adma.201701392>.
22. A. Ajmal, I. Majeed, R.N. Malik, H. Idriss and M.A. Nadeem, *RSC Advances*, **4**, 37003 (2014); <https://doi.org/10.1039/C4RA06658H>.
23. A.K. Subramani, K. Byrappa, S. Ananda, K.M. Lokanatha Rai, C. Ranganathaiah and M. Yoshimura, *Bull. Mater. Sci.*, **30**, 37 (2007); <https://doi.org/10.1007/s12034-007-0007-8>.
24. S. Barisci, H. Inan, O. Turkey, A. Dimoglo and D. Erol, *J. Appl. Solut. Chem. Model.*, **6**, 75 (2017); <https://doi.org/10.6000/1929-5030.2017.06.02.3>.
25. H. Zeng, X. Liu, T. Wei, X. Li, T. Liu, X. Min, Q. Zhu, X. Zhao and J. Li, *RSC Adv.*, **7**, 23787 (2017); <https://doi.org/10.1039/C7RA02761C>.
26. L.C. Yang, Q.S. Gao, Y. Tang, Y.P. Wu and R. Holze, *J. Power Sources*, **179**, 357 (2008); <https://doi.org/10.1016/j.jpowsour.2007.12.099>.
27. R.S. Patil, M.D. Uplane and P.S. Patil, *Appl. Surf. Sci.*, **252**, 8050 (2006); <https://doi.org/10.1016/j.apsusc.2005.10.016>.
28. N. Dukstiene, L. Tatariskinaite and M. Andrulevicius, *Mater. Sci.-Poland*, **28**, 93 (2010).
29. Z. Liang, *Stochastic Anal. Appl.*, **24**, 501 (2006); <https://doi.org/10.1080/07362990600629017>.
30. J. Bi, C. Yang and H. Wu, *Ceram. Int.*, **43**, 92 (2017); <https://doi.org/10.1016/j.ceramint.2016.09.115>.
31. D. Kandi, S. Martha, A. Thirumurugan and K.M. Parida, *J. Phys. Chem. C*, **121**, 4834 (2017); <https://doi.org/10.1021/acs.jpcc.6b11938>.
32. K.M. Reza, A.W.S. Kurny and F. Gulshan, *Appl. Water Sci.*, **7**, 1569 (2017); <https://doi.org/10.1007/s13201-015-0367-y>.
33. A. Hezam, K. Namratha, Q.A. Drmosh, B.N. Chandrashekar, G.K. Jayaprakash, C. Cheng, S.S. Swamy and K. Byrappa, *Ceram. Int.*, **44**, 7202 (2018); <https://doi.org/10.1016/j.ceramint.2018.01.167>.
34. K.R. Raksha, S. Ananda and N.M. Madegowda, *J. Mol. Catal. Chem.*, **396**, 319 (2015); <https://doi.org/10.1016/j.molcata.2014.10.005>.